IOP Conf. Series: Materials Science and Engineering **1345** (2026) 012017 doi:10.1088/1757-899X/1345/1/012017

FEM Modelling of Current Sharing in Tape Stack Cables; Influence of ICR, ITR, Defect Number, Defect Patterns, and Thermal Boundary Conditions

Minzheng Jiang[1], Milan Majoros[1], Edward W. Collings[1], and Mike D. Sumption[1]

[1]Department of MSE, Ohio State University, Columbus, USA

E-mail: jiang.1535@osu.edu

Abstract

In previous current sharing simulation studies, we showed that a current sharing ratio can be defined, and that it is inversely proportional to the number of defects in the cable. We also gave a specific function for this, for a given set of boundary conditions, defect pattern, and thermal and electrical parameters. In this work, we explore the relationship between the current sharing ratio and different patterns of defects. A COMSOL simulation model, a four-tape stack model was used; a simple stack of tapes (a "carpet stack" or tape stack cable). The center two tapes had three pre-existing defects each, and each defect was 0.1 mm I n length with a critical current density of $0.1J_c$. The defects in the center tapes were arranged either (i) at three equally spaced lengths along the stack length, but the same lengthwise position in both tapes ("column" pattern) or (ii) with the defects in the second tape positioned halfway between the lengthwise positions of those of the first tape ("zig-zag" pattern). The cable was modelled as being fully immersed in liquid helium. A stationary model was employed using an error tolerance of 1e-3 with a fine physics-controlled mesh. Other important parameters include an interstrand contact resistance (ICR) = 5400μΩ*cm^2 and an Interstrand thermal resistance (ITR) = 5.54 K*m^2/W. Results show that the zig-zag defect pattern allows a higher current sharing ratio.

1. Introduction

Superconducting tapes, especially rare-earth barium copper oxide (ReBCO) based coated conductors (cc), [1][2] have significant potential in high-field magnet systems for applications in energy storage, medical imaging, and high-energy physics (HEP) accelerator magnets [3][4][5] due to their exceptional current-carrying capabilities under high magnetic fields. Defects can occur in tapes and cables made from them, but current sharing between tapes (if present) mitigate the effects of such defects that might otherwise limit performance. Thus, understanding

Content from this work may be used under the terms of the Creative Commons Attribution 4.0 licence. Any further distribution of this work must maintain attribution to the author(s) and the title of the work, journal citation and DOI.
Published under licence by IOP Publishing Ltd

current sharing, i.e. the redistribution of current between adjacent superconducting tapes to bypass local defects, and its systematics is crucial to improving cable reliability and reducing the risks associated with thermal runaway and quenching phenomena. [6][7]

Previous finite element method (FEM) simulation studies conducted using COMSOL Multiphysics have established that both the presence and quantity of defects influence the current sharing ratio (CSR), [7][8] which we can define as the achievable ratio of critical current in defected cable (I_{cable_defect}) to that of a defect-free cable ($I_{cable\_no\_defect}$) just before thermal runaway. Previous work quantified (for a very specific simple cable structure) the functional form of the functional dependence of CSR with defect density [8]. While more general application to realistic cables is required, we also need to examine how the distribution of defects affects CSR. So, working again with our simple model, this study expands the investigation to explore the impact of different defect distribution patterns, collinear (column) and laterally displaced (zig-zag) arrangements on the current sharing capabilities within multi-layer tape stack cables.

The simulation model is a four-tape stack cable, representing a simplified realistic geometry, including copper, $YBa_2Cu_3O_{7-x}$ (YBCO), buffer, and Hastelloy layers. Each pattern studied includes three pre-existing defects in two tapes (six defects total) characterized by significantly reduced critical current densities. [7][8][9][10] The cable's thermal and electrical responses are evaluated under steady-state conditions with set Interstrand contact resistances (ICR) and interstrand thermal resistances (ITR) as well as prescribed thermal boundary conditions. By systematically varying the defect pattern, the research aims to identify differences in thermal and electrical behavior induced by the defect patterns, which could aid the development of optimized superconducting cables for demanding applications in high-field magnet technology.

2. The Model

We used COMSOL Multiphysics software for the 3D FEM modelling of the cable. The model had both the electrostatic and temperature components, and we performed a series of steady state simulations for various values of I/I_c, observing the resulting steady state temperature up until the last stable point before thermal runaway. Our four-tape stack model assumed a simple stack of tapes (a “carpet stack” [11] or tape stack cable). The width of the tape (and cable) was 4 mm, and the cable had a total length of 3 cm, with six to three pre-existing defects evenly spaced along the central tape [10] [12]. In this study, the defect had a length of 0.1 mm, was present across the entire tape width, and had a critical current density of $0.1J_c$, see Figure 1. In our model each tape consisted of a Hastelloy substrate, on top of which (after the buffer layer) a 5 μm ReBCO layer was present. To capture the properties of the buffer layers, we set the interface between REBCO layer and the Hastelloy to be an insulating interface. Surrounding this, a 20 μm depth of copper stabilizer was present on the top, bottom and side surfaces. The Ag cap layer on the ReBCO is very thin and it was thus possible to neglect it in our models. Further details are presented in Table I, and a simple schematic geometric model of the cable is shown in Figure 1.

Table I: Tape Details

Width of REBCO	4 mm
Thickness of Cu	20 μm
Thickness of Hastelloy	30 μm
Thickness of REBCO	5 μm
Length of tape	3 cm
Length of defect	0.1 mm
RRR value of Cu	100
n-value	15
I_c (4.2K, 8T)	596 A
J_c(4.2K, 8T)	$2.98*10^{10}$ A/m^2

Figure 1 shows the structure of the four-tape stack cable where the middle two tapes have defects, and the top and bottom tapes have no defect. Voltages were applied at the end of the cable as shown (circled) in Figure 1, and the other end was grounded. The current flows from the positive terminal to ground. An equipotential was applied to all three tapes at each terminal (respectively), while a potential difference was applied between the terminals. The inset shows the structure of the cable with defect. This correlates to a defect which is present in the cable before excitation (created during either conductor or cable fabrication, or during a previous magnet excitation cycle).

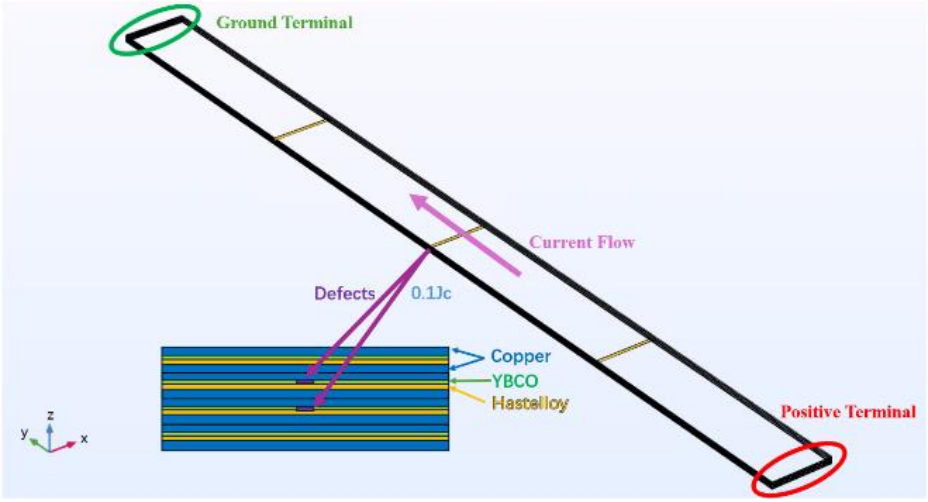

Figure 1. Geometry of the four-layer Tape Stack Cable. The orange (purple in inset) regions are the defects. The terminals are circled, the current flows from the positive terminal to the ground. An equipotential was applied to all four tapes at each terminal (respectively), while a potential difference was applied between the terminals. The inset shows the structure of the cable with defect.

Heat transfer in the longitudinal direction was governed by the thermal conductivities of REBCO, Hastelloy, and copper as shown in Figure 1. The terminal (cable end) surfaces were defined as electrically conductive but thermally insulating following [13] [14] [15]. The superconductor was modelled as a power law conductor with $J = \sigma E$, $E = E_c\,(I/I_c)^n$, and $n = 15$, following [16] (as might be expected at high fields, our region of interest). The critical current was temperature dependent

[16] following $J_c = J_{c0}$ (1-T/T_c). Since in our case all simulations were performed with conductor properties as they might be found in moderately high fields (e.g., 8 T). The J_c values chosen are illustrative and typical, rather than attempting to represent a particular conductor in a particular magnet.

Figures 2 and 4 are the 3D view of the column pattern cable and the zig-zag pattern cable. The defects of column pattern cable are placed at specific positions (the same positions) equally spaced along the length in the middle two tapes. Defects overlay in the middle two layers of tape shown in Figure 3 as the side view. The defects of the zig-zag pattern cable are uniformly placed in the middle two layers of the cable as down-up-down-up-down-up style, shown as Figure 5.

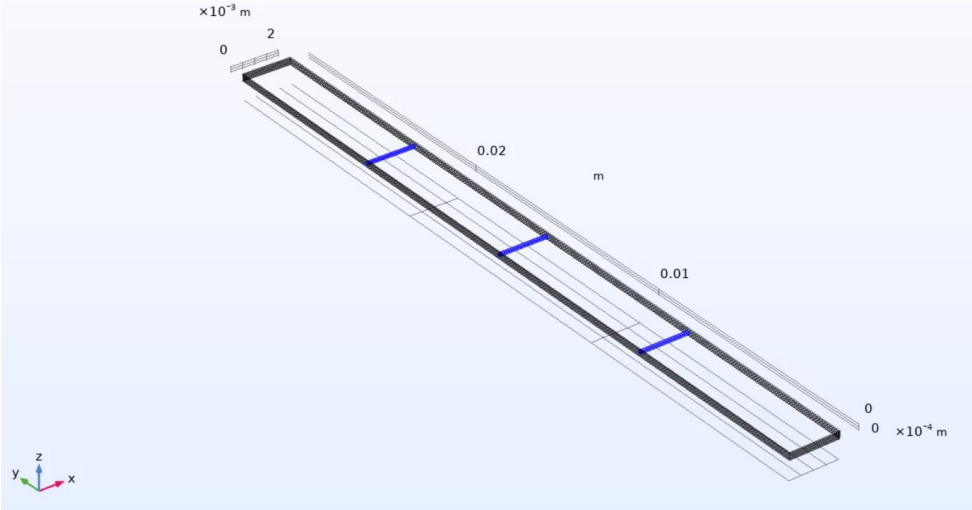

Figure 2. 3D view of the column pattern cable, the blue lines on the cable are the defects.

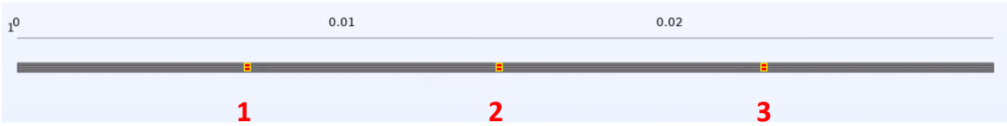

Figure 3. Side view of the column pattern cable; the yellow/red blocks are the defects.

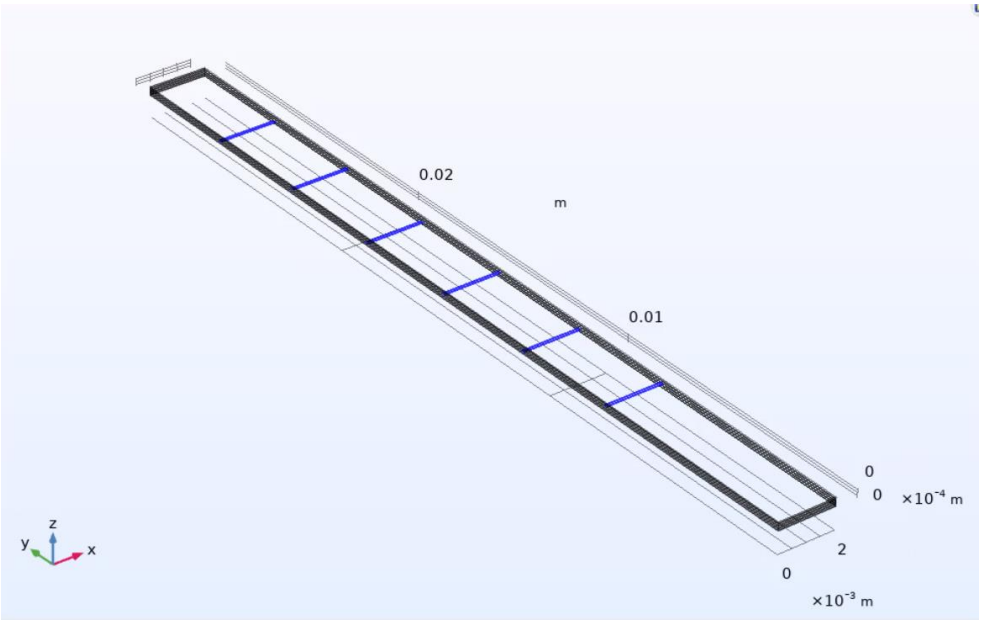

Figure 4. 3D view of the zig-zag pattern cable, the blue lines on the cable are the defects

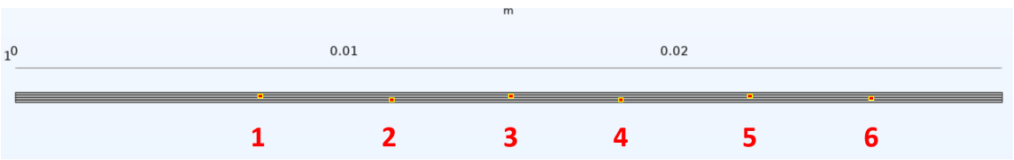

Figure 5. The graph shown the side view of the zig-zag pattern cable. The yellow/red blocks are the defects

In addition to the thermal boundary conditions on the cable, the nature of the tape-to-tape interfaces (and tape internal structure) play a crucial role in determining heat dissipation and current sharing within stacked superconducting tapes. The ICR and ITR between adjacent tapes, as well as the effective thermal and electrical conductance within the tape, directly affect the local temperature distribution and current path. Stacking pattern, such as alternating placement of defects overlap or not, requires additional consideration. Compared with columnar pattern defects, the alternating stacking (zigzag) pattern can allow current to avoid the defects, as well as significantly spread the heat load and promote better heat dissipation to alleviate local hot spots and delay thermal runaway. Therefore, paying attention to the boundary layer characteristics and defect stacking patterns is crucial to optimize the thermal stability and performance reliability of superconducting cable systems.

In this work we use an inter-tape contact efficiency, η, of 5400 $\mu\Omega*cm^2$ (η =inter-strand contact resistance (ICR)*contact area) and an inter-tape thermal resistance, ω, of 5.54 $K*m^2/W$ [17] (ω= ITR*contact area). Both η and ω are interfacial parameters, that is, properties of the surfaces between the tapes. The internal resistances (thermal and electrical) of the Hastelloy and Cu are considered those of isotropic bulk materials properties and taken from the COMSOL database (a Cu RRR = 100 is assumed) [18]. The influence of the buffer layer is again an interfacial resistance (thermal and electrical) taken as in fact insulating. The FEM model included a fine mesh where the final geometry consisted of 159437 domain elements, 64446 boundary elements, and

7351 edge elements. The number of degrees of freedom (DOF) solved was 1,104,442 (plus 260,714 internal DOFs). The solvers were set as stationary and set up automatically by the Comsol Multiphysics software. The physics-controlled mesh was set as "fine". The stationary solver tolerance setting was set at 1e-3 for these simulations.

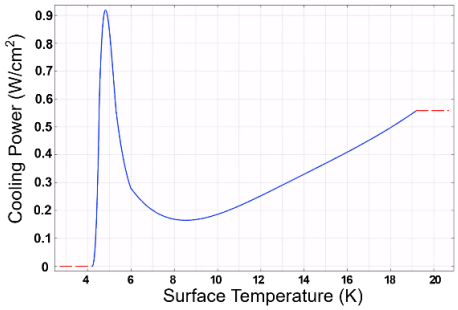

Figure 6. The liquid helium pool cooling curve.

We define the thermal boundary conditions to be pool boiling liquid helium on all surfaces of the cable shown as Figure 6. In this simulation, we used the liquid helium pool boiling curve to define the cooling power (related to the heat transfer coefficient) at the surface of the cable as a function of the surface temperature. [14][19] That is, the simulation found a locally self-consistent solution for the cooling power and temperature. We note that the nucleate boiling peak temperature is 4.535 K, for temperatures above this, the system will transfer from the nucleate boiling to the film boiling regime, accompanied by a huge decrease in the cooling power. As noted above we have defined current sharing is defined as the achievable ratio of $I_{cable\_defect}/I_{cable\_no\_defect}$ (I/I_c) that occurs just before thermal runaway. Given the shape of the pool boiling curve, thermal runaway is often associated with a temperature near the nucleate to film boiling transition.

3. Results and Discussion

Our simulations evaluated the thermal and electrical response of a four-tape stack superconducting ReBCO cable subjected to two distinct defect patterns: collinear (column) and laterally displaced (zig-zag). Each inner tape had three evenly spaced defects, but the defects of the bottom tape were shifted such that they occurred mid-way between the defects of the upper of the two defected tapes. Each defect had a reduced critical current density of $0.1J_c$. In all cases we assumed that the surfaces of the cables were exposed to liquid helium, providing uniform thermal boundary conditions defined by pool boiling characteristics.

Figs. 7 and 8 show the temperature distribution profiles of the cable under steady-state conditions for both defect patterns. The simulation results demonstrate the localization of hotspots around defect regions in both the column and zig-zag arrangements. In the columnar pattern (Figure 7), defects aligned longitudinally one atop another causes the hot spots to be concentrated in one line which promoting direct heat accumulation along the defect axis. In contrast, the zig-zag pattern (Figure 8) exhibits laterally dispersed hot spots, resulting in a more distributed thermal load over the cable cross-sectional area.

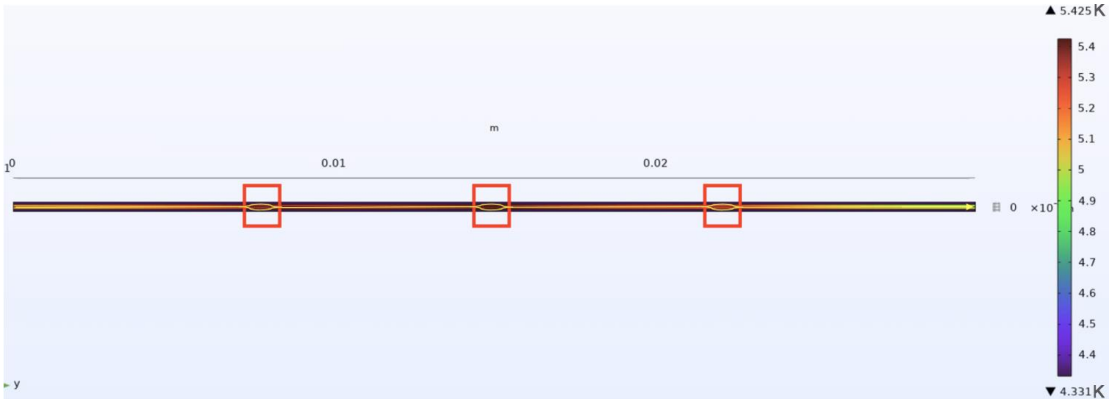

Figure 7. The bigger view of temperature graph for column defect pattern. The middle defect column has a higher temperature than the side columns. The yellow line is the current flow direction.

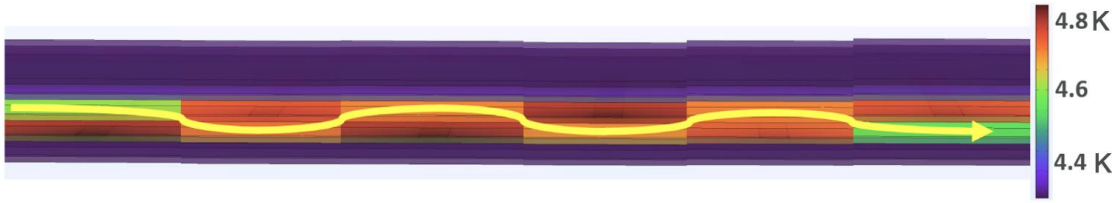

Figure 8. The bigger view of temperature graph for the zig-zag defect pattern. The defect parts of the cable have higher temperature, and the no-defect parts have lower temperature. The yellow arrow is the current flow direction. With I/I_c is 0.887, ICR=5400 μΩ∗cm², ITR= 5.54 K∗m²/W.

At lower transmission currents, the initial hotspot temperatures of both patterns are similar, but deviations become apparent as the current approaches the thermal runaway threshold. Specifically, the zig-zag pattern exhibits superior thermal management capabilities due to the spatial dispersion of heat, which delays the onset of thermal instability compared to the columnar pattern. The cut plane *y-z* in Figure 9 is actually the central plane of the tape. The blue arrow is from YBCO to copper layer and the green arrow is from the copper layer to the YBCO layer.

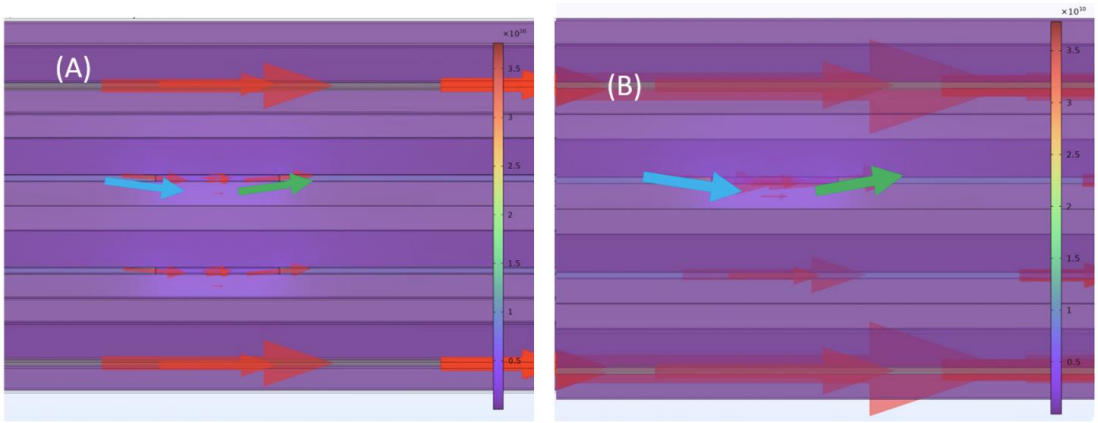

Figure 9. Current density with current flow direction about a defect of (A) column pattern (B) zig zag pattern. Larger red arrows mean larger current density. Here we have set η = 5400 μΩ∗cm², ω= 5.54 K∗m²/W, and used the thermal boundary conditions of pool boiling liquid helium on the surface of the cable.

Figure 10 compares the maximum transport current achievable before thermal runaway for both defect patterns. The zig-zag defect pattern consistently allows for higher transmission current, with an improved current sharing ratio compared to the collinear structure. Quantitative analysis shows that under the same simulation conditions, the zig-zag pattern allows the cable to withstand approximately 5% to 10% additional current load before thermal runaway occurs.

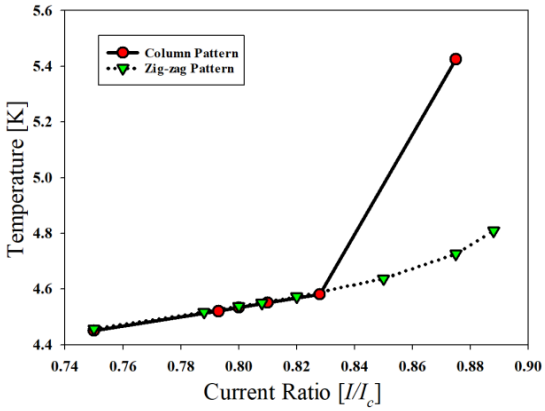

Figure 10. The zig-zag pattern of defects can load more current than column pattern.

The enhanced performance observed in the zig-zag configuration arises primarily from its ability to distribute current pathways around localized defects more effectively. In contrast, the column pattern, with defects aligned centrally, presented fewer alternative conduction paths, intensifying localized heating and thus precipitating earlier thermal runaway.

The cooling characteristics of liquid helium significantly impacted the current sharing and thermal stability behaviors observed. Near the transition from nucleate boiling to film boiling (~4.535 K), a slight increase in temperature significantly reduces the cooling efficiency and exacerbates thermal instabilities. Therefore, the column pattern defects concentrate the heat along a linear path, thus inducing a faster transition from nucleate boiling to film boiling.

Furthermore, the interaction between closely spaced defects in the column pattern intensifies the local heating and accelerates the onset of thermal runaway. In the zig-zag pattern, the spatial separation between defects reduces the cumulative thermal interaction, thereby mitigating excessive temperature rise and enhancing the cable's ability to maintain stable operation at higher transmission currents.

4. Summary and Conclusion

This study used finite element modeling to investigate how different defect arrangements affect current sharing in a four-tape YBCO superconducting cable. Two defect patterns were analyzed: column pattern (defects at the same lengthwise position along the cable) and zig-zag pattern (staggered defects). Both configurations involved identical defect properties and were modeled under steady-state conditions in a liquid helium bath, with ICR= 5400 $\mu\Omega*cm^2$, ITR= 5.54 $K*m^2/W$.

Simulation results showed that although both patterns developed hotspots around defect regions, the zig-zag arrangement led to better thermal distribution and a delayed the onset of quench (as compared to the column pattern). It allowed the cable to carry 5–10% more current before thermal runaway compared to the column configuration. This improvement is due to more effective redistribution of current paths and reduced thermal interaction between defects.

The study also confirmed that thermal boundary conditions, especially near the liquid helium boiling transition at ~4.535 K, play a critical role in determining the quench point. Defects that are closely aligned (as in the column pattern) promote faster heating and reduced cooling efficiency.

In practice, this suggests that a random distribution of defects, as might result from cabling strands with inevitable manufacturing variations are less limiting in terms of current sharing than correlated defects, as might happen if a cable experiences either localized or spatially periodic damage either during magnet winding or operation. Our next steps include exploring a more randomized distribution of defects, both in terms of spatial distribution, as well as strength.

Acknowledgements

This work was supported by the U.S. Department of Energy, Office of Science, Division of High Energy Physics, under Grant DE SC0011721.

References

[1] Vetrella U B, Celentano G, Marchetti M, Messina G, Morici L, Sabatino P, Viola R and della Corte A 2014 HTS coils fabrication from commercial 2G YBCO tapes: measurements and simulation *IEEE Trans. Appl. Supercond.* **24** 1–4

[2] Pei R, Velichko A, Majoros M, Jiang Y, Viznichenko R, Hong Z, Marchant R, Campbell A M and Coombs T A 2008 Ic and AC loss of 2G YBCO tape measurement for designing and fabrication of an HTS motor *IEEE Trans. Appl. Supercond.* **18** 1236–1239

[3] Koyanagi K, Tosaka T, Tasaki K, Kurusu T, Yoshiyuki T, Amemiya N and Ogitsu T 2012 Fabrication of YBCO small test coils for accelerator magnet development *IEEE Trans. Appl. Supercond.* **22** 4101904

[4] Salama A H, Youssef A M, Rammah Y S and El-Khatib M 2019 YBCO as a transition metal oxide ceramic material for energy storage *Bull. Natl. Res. Centre* **43** 89

[5] Parkinson B J, Slade R, Mallett M J and Chamritski V 2013 Development of a cryogen-free 1.5 T YBCO HTS magnet for MRI *IEEE Trans. Appl. Supercond.* **23** 4400405

[6] Marchevsky M and Prestemon S 2024 Thermal runaway criterion as a basis for the protection of high-temperature superconductor magnets *Supercond. Sci. Technol.* **37** 035012

[7] Xue S, Majoros M, Sumption M D, Garg T and Collings E W 2023 FEM analysis of current sharing in ReBCO coated-conductor cables for particle accelerator applications *IEEE Trans. Appl. Supercond.* **33** 1–7

[8] Jiang M, Xue S, Majoros M, Collings E W and Sumption M D 2025 FEM modeling of current sharing in tape stack cables: influence of ICR, ITR, defect number, and thermal boundary conditions *IEEE Trans. Appl. Supercond.* **35** 1–5

[9] Majoros M, Sumption M D, Xue S and Collings E W 2024 Current sharing in superconducting ReBCO cables—FEM modeling *IEEE Trans. Appl. Supercond.* **34** 1–5

[10] Majoros M, Sumption M D, Xue S and Collings E W 2022 Stability and current sharing in YBCO cables: impact of broken elements—FEM modeling *IEEE Trans. Appl. Supercond.* **32** 1–5

[11] Ekin J W 2006 Critical-current measurements *Experimental Techniques for Low-Temperature Measurements* (Oxford: Oxford University Press) pp 353–394

[12] Majoros M, Sumption M D, Collings E W and Long N J 2015 Inter-strand current sharing and AC loss measurements in superconducting YBCO Roebel cables *Supercond. Sci. Technol.* **28** 055010

[13] Grissonnanche G, Cyr-Choinière O, Laliberté F, René de Cotret S, Juneau-Fecteau A et al 2014 Direct measurement of the upper critical field in cuprate superconductors *Nat. Commun.* **5** 3280

[14] Berger A D 2011 *Stability of superconducting cables with twisted stacked YBCO coated conductors* MSc Thesis (Massachusetts Institute of Technology) Available at: https://dspace.mit.edu/handle/1721.1/93343 (accessed 10 May 2025)

[15] Ekin J W 2015 *Experimental Techniques for Low-Temperature Measurements: Cryostat Design, Material Properties, and Superconductor Critical-Current Testing* (Oxford: Oxford University Press)

[16] Majoros M, Sumption M D and Collings E W 2022 Dipole magnets wound using YBCO cables: FEM stability-issues modeling *IEEE Trans. Appl. Supercond.* **32** 1–5

[17] Xue S, Sumption M D and Collings E W 2021 YBCO coated-conductor interlayer electrical contact resistance measured from 77 K to 4 K under applied pressures up to 9.4 MPa *IEEE Trans. Appl. Supercond.* **31** 1–5

[18] Fouaidy M and Hammoudi N 2006 RRR of copper coating and low-temperature electrical resistivity of material for TTF couplers *Physica C* **441** 137–144

[19] Brentari E G 1965 Boiling heat transfer for oxygen, nitrogen, hydrogen and helium US National Bureau of Standards **13**